



This is a repository copy of *Localised turbulence in a circular pipe flow with gradual expansion*.

White Rose Research Online URL for this paper:
<http://eprints.whiterose.ac.uk/85947/>

Version: Accepted Version

Article:

Selvam, K., Peixinho, J. and Willis, A.P. (2015) Localised turbulence in a circular pipe flow with gradual expansion. *Journal of Fluid Mechanics*, 771. ISSN 0022-1120

<https://doi.org/10.1017/jfm.2015.207>

Reuse

Unless indicated otherwise, fulltext items are protected by copyright with all rights reserved. The copyright exception in section 29 of the Copyright, Designs and Patents Act 1988 allows the making of a single copy solely for the purpose of non-commercial research or private study within the limits of fair dealing. The publisher or other rights-holder may allow further reproduction and re-use of this version - refer to the White Rose Research Online record for this item. Where records identify the publisher as the copyright holder, users can verify any specific terms of use on the publisher's website.

Takedown

If you consider content in White Rose Research Online to be in breach of UK law, please notify us by emailing eprints@whiterose.ac.uk including the URL of the record and the reason for the withdrawal request.



eprints@whiterose.ac.uk
<https://eprints.whiterose.ac.uk/>

Localised turbulence in a circular pipe flow with gradual expansion

Kamal Selvam¹, Jorge Peixinho^{1†} and Ashley P. Willis²

¹Laboratoire Ondes et Milieux Complexes, CNRS & Normandie Université
53 rue de Prony, 76600 Le Havre, France

²School of Mathematics and Statistics, University of Sheffield, Sheffield S3 7RH, UK

(Received 13 May 2015)

We report the results of three-dimensional direct numerical simulations for incompressible viscous fluid in a circular pipe flow with a gradual expansion. At the inlet, a parabolic velocity profile is applied together with a constant finite amplitude perturbation to represent experimental imperfections. Initially, at low Reynolds number, the solution is steady. As the Reynolds number is increased, the length of the recirculation region near the wall grows linearly. Then, at a critical Reynolds number, a symmetry-breaking bifurcation occurs, where linear growth of asymmetry is observed. Near the point of transition to turbulence, the flow experiences oscillations due to a shear layer instability for a narrow range of Reynolds numbers. At higher Reynolds numbers the recirculation region breaks into a turbulent state that remains spatially localised and unchanged when the perturbation is removed from the flow. Spatial correlation analysis suggests that the localised turbulence in the gradual expansion possess a different flow structure from the turbulent puff of uniform pipe flow.

1. Introduction

In the axisymmetric sudden-expansion pipe flow, bifurcations of flow patterns have been studied experimentally (Sreenivasan & Strykowski 1983; Latornell & Pollard 1986; Hammad *et al.* 1999; Mullin *et al.* 2009) and numerically (Sanmiguel-Rojas *et al.* 2010; Sanmiguel-Rojas & Mullin 2012). In these studies, flow separation after the expansion and reattachment downstream leads to the formation of a recirculation region near the wall. Its extent grows linearly as the flow velocity is increased. Numerical simulations and experimental results have shown that the recirculation region breaks symmetry once a critical Reynolds number is exceeded. Here, the Reynolds number Re is defined as $Re = Ud/\nu$, where U is the bulk flow velocity, d is the inlet diameter and ν is the kinematic viscosity. In experiments, the recirculation region loses symmetry at $Re \simeq 1139$ (Mullin *et al.* 2009) and then breaks to form localised turbulence that tends to remain in the same spatial position (Sreenivasan & Strykowski 1983). In terms of global stability analysis, Sanmiguel-Rojas *et al.* (2010) have shown that the symmetry breaking occurs after a critical Reynolds number of ≈ 3273 . The reason for the early occurrence of transition is believed to be due to experimental imperfections. Numerical simulations with an applied finite amplitude perturbation (Sanmiguel-Rojas & Mullin 2012) found the transition to turbulence to occur at $Re \gtrsim 1500$, which depends upon the amplitude of the perturbation.

† Email address for correspondence: jorge.peixinho@univ-lehavre.fr

The goal of the present investigation is to numerically model the gradual expansion (diverging) pipe flow with an imperfection added to the system that could trigger early transition to turbulence. The long term motivation of this study is to understand the effect of the diverging angle on the transition to turbulence. In the first part, the numerical method and its validation are presented. In the second part, the results for the asymmetric growth of the recirculation are discussed, along with the oscillation of the flow, the time evolution of the localised turbulence, and observations of decay of the turbulent structure.

2. Numerical method

The solutions are obtained by solving the unsteady three-dimensional incompressible Navier-Stokes equation for a viscous Newtonian fluid:

$$\nabla \cdot \mathbf{v} = 0 \quad (2.1)$$

$$\frac{\partial \mathbf{v}}{\partial t} + \mathbf{v} \cdot \nabla \mathbf{v} = -\nabla P + \frac{1}{Re} \nabla^2 \mathbf{v}, \quad (2.2)$$

where $\mathbf{v} = (u, v, w)$ and P denote the scaled velocity vector and pressure respectively. The equations (2.1) and (2.2) were non-dimensionalised using the inlet pipe diameter, d , for the length scale and the bulk velocity at the inlet, U , for the velocity scale. The time scale and the pressure scale are therefore $t = d/U$ and ρU^2 , where ρ is the density of the fluid. The equations are solved with the boundary conditions:

$$\mathbf{v}(\mathbf{x}, t) = 2(1 - 4r^2)\mathbf{e}_z \quad \mathbf{x} \in Inlet, \quad (2.3)$$

$$\mathbf{v}(\mathbf{x}, t) = 0 \quad \mathbf{x} \in Wall, \quad (2.4)$$

$$P\mathbf{n} - \mathbf{n} \cdot \nabla \mathbf{v}(\mathbf{x}, t)/Re = 0 \quad \mathbf{x} \in Outlet, \quad (2.5)$$

corresponding to a fully developed Hagen-Poiseuille flow (2.3) at the inlet, no-slip (2.4) at the walls, and an open boundary condition (2.5) at the outlet of the pipe. Equation (2.5) enforces Neumann boundary conditions in weak sense for the velocity components, which minimises the possibility of numerical oscillations and reflections of outgoing waves, where \mathbf{n} is the normal surface vector directed out of the computational domain. The equations were solved using an open source code nek5000 developed by Fischer *et al.* (2008). Spatial discretisation is based on the spectral element method using Lagrange polynomials. The equations are reduced to a weak form and discretised in space by Galerkin approximation. N^{th} order Lagrange polynomial interpolants on Gauss-Lobatto-Legendre points were chosen as the basis for the velocity space, similarly for the pressure space. In all the simulations $\mathbb{P}_N - \mathbb{P}_N$ formulations were implemented, which denotes that the same polynomial order was used for both velocity and pressure. The time-stepping in nek5000 is semi-implicit in which the viscous term of the Navier-Stokes equations are treated implicitly using third order backward differentiation and the non-linear terms are treated by a third order extrapolation scheme (Fischer *et al.* 2008; Maday *et al.* 1990).

Figure 1 shows the geometry of the divergent pipe along with the mesh. It consists of three parts (1) the inlet, (2) the diverging section and (3) the outlet. The velocity field is simulated in the Cartesian coordinate system (x, y, z) . The expansion ratio is $E = D/d = 2$, where D is the outlet pipe diameter. The length of the divergent section is kept constant in this study and of length d , which leads to a divergence half-angle $\alpha = 26.57^\circ$. The length of the inlet pipe is $5d$ and the outlet pipe length is $150d$.

The mesh was developed using hexahedral elements with a non-uniform growth rate. It contains 80 elements with refinement near the wall in the (x, y) cross-section and 180 elements in the z direction. A refinement has been applied in the diverging section as

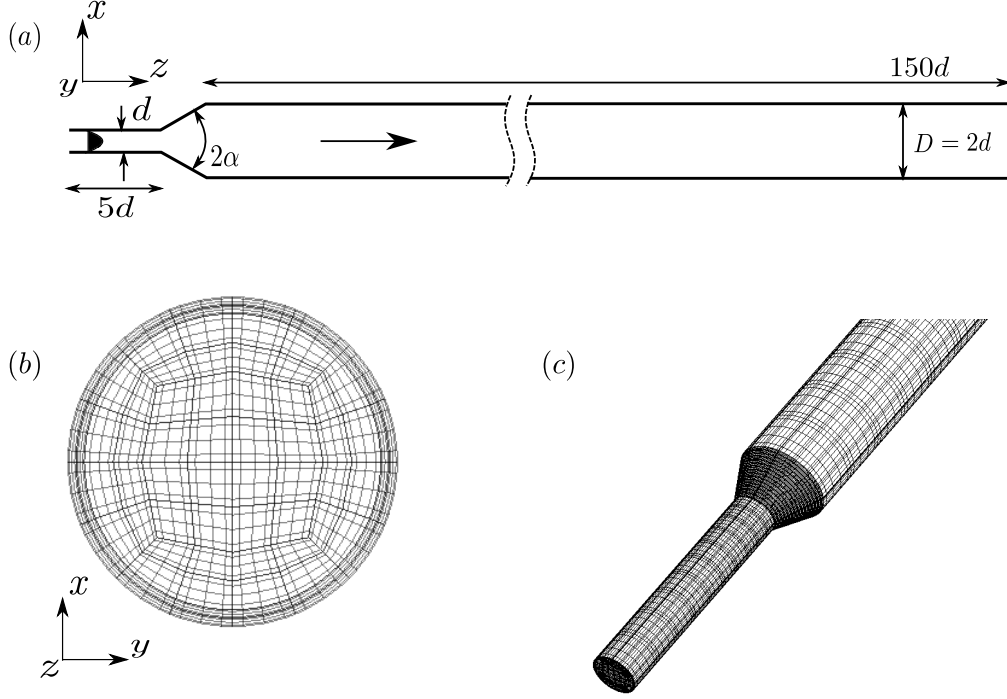


FIGURE 1. The spectral-element mesh used in the present study with a divergent angle of $\alpha = 26.57^\circ$. (a) Sketch of the domain, (b) cross-section of the mesh (dark lines represent the elements and the grey lines represent the Gauss-Lobatto-Legendre points) and (c) a three-dimensional view of the mesh near the diverging section. The mesh is made of $K = 14\,400$ elements.

shown in figure 1(c) in order to resolve the flow separation. The streamwise extent of the elements increases along z in the outlet section. The total number of grid points in the simulation is approximately KN^3 , where K is the number of elements and N is the polynomial order. The flow was initialised with fully-developed Poiseuille in the inlet section and each simulations were computed using 512 cores. Table 1 shows the length of the recirculation region for different orders of polynomial at $Re = 1000$. The mesh convergence study was carried out by changing the polynomial order N of the Lagrange polynomial, of the spectral elements. The observations used to assess convergence are the flow reattachment point, z_r , and the viscous drag $(\rho U^2/2)\mathcal{A}_w C_f$, where \mathcal{A}_w is the surface area of the outlet pipe wall and C_f is the friction coefficient. The length of the recirculation region depends sensitively on the resolution of the separated shear layer, particularly near the separation point. The polynomial order of $N = 5$ is sufficient to resolve the flow accurately. This value of N and the mesh have been used in all the following simulations, which corresponds to $KN^3 \approx 1.8 \times 10^6$ grid points.

To validate further the simulations at higher Reynolds number, the growth of the recirculation region as a function of the Reynolds number is shown in figure 2. The simulations show that the extent of the recirculation region is of the form $2z_r = 0.0866Re$, which agrees well with previous studies for sudden expansion flow. Unlike the sudden expansion flow, for a divergent pipe, the recirculation is formed after a critical flow velocity, shown in the inset to figure 2, which depends upon the divergence half-angle α and Re (Peixinho & Besnard 2013).

N	Reattachment Position z_r	Viscous Drag
3	43.68	0.8430
4	43.65	0.3566
5	43.58	0.3419
6	43.59	0.3418
7	43.58	0.3419

TABLE 1. Convergence study, changing the order of polynomial N . z_r is the non-dimensional length of the recirculation region in the pipe for $Re = 1000$.

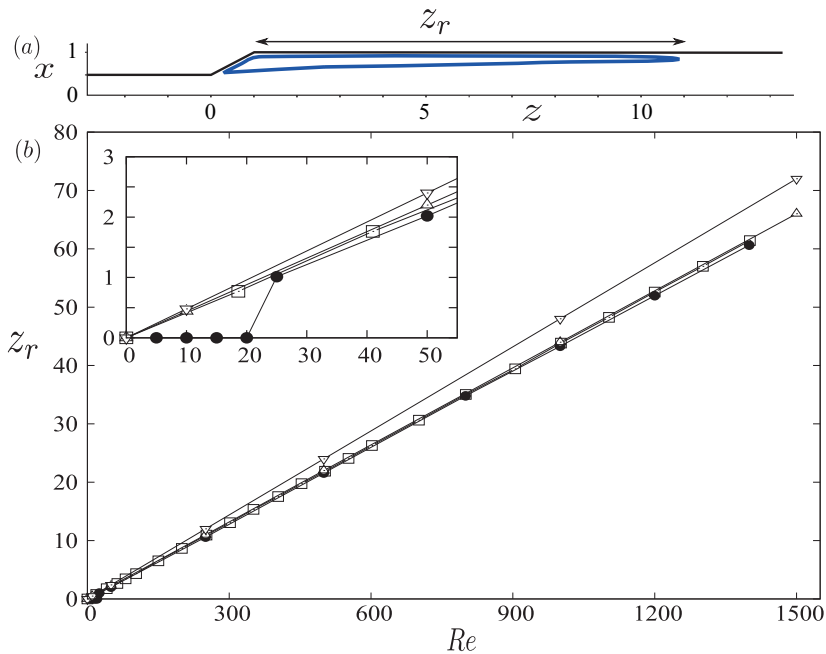


FIGURE 2. (a) Streamline of the recirculation region of length z_r inside the diverging pipe at $Re = 300$. (b) Recirculation region length, z_r , with respect to Re . (●) corresponds to best-fit proportionality given by $2z_r = 0.0866Re$ for present case. (□) corresponds to $2z_r = 0.0874Re$ (Cantwell *et al.* 2010), (Δ) and (∇) corresponds to experimental result (Latornell & Pollard 1986; Hammad *et al.* 1999) $2z_r = 0.088 Re$ and $2z_r = 0.096Re$ respectively for sudden expansions.

3. Results and discussion

For sudden expansion pipe flow, numerical simulations (Cantwell *et al.* 2010; Sanmiguel-Rojas *et al.* 2010) have shown that the flow is unstable to infinitesimal perturbations for $Re \approx 3273$, but the transition in experiments occurs at much lower Re (Sreenivasan & Strykowski 1983; Latornell & Pollard 1986; Mullin *et al.* 2009). The exact nature of the observed instability is therefore unclear. Small disturbances in an experimental setup are likely to be amplified due to the convective instability mechanism, and appear to be necessary to realise time-dependent solutions. Numerical results (Cantwell *et al.* 2010), have shown that small perturbations are amplified by transient growth in the sudden expansion for $Re \leq 1200$, advect downstream and decays. Here, the initial simulations

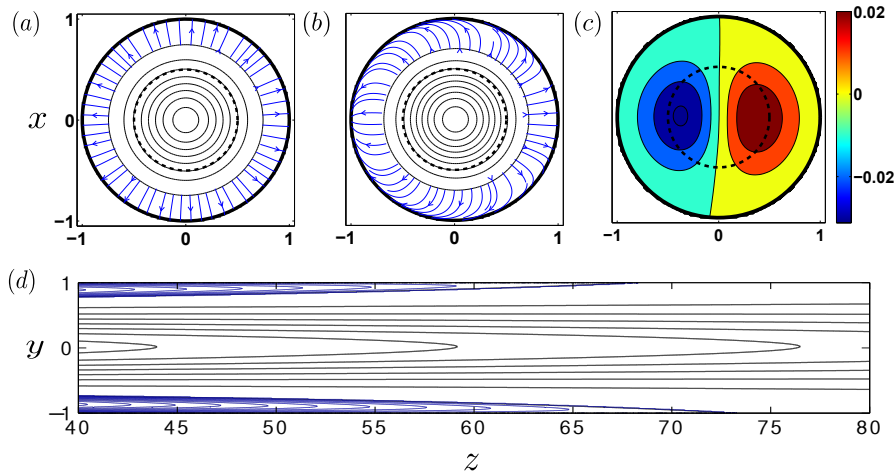


FIGURE 3. Cross-sections of the pipe. Contour line plots of the axial velocity (solid black lines) taken at $z = 22.5$ for (a) $Re = 1000$ and (b) $Re = 1600$. The dashed line corresponds to the inlet pipe diameter and the blue lines with arrows represent the crosswise velocities within the recirculation region. (c) Contour plot of the perturbation, i.e., flow with perturbation ($\delta = 0.001$) subtracted from the base flow ($\delta = 0$) for $Re = 1600$. (d) Streamwise cross-section of the flow around the reattachment point at $Re = 1600$ with $\delta = 0.001$.

showed that the flow is linearly stable for upto $Re \gtrsim 2200$ for the present computational domain. For larger Re the recirculation bubble extends close to the end of the outlet section and cannot be calculated reliably. In order to induce early transition a disturbance is applied to the numerical system in the form (Sanmiguel-Rojas & Mullin 2012):

$$u(\mathbf{x}, t) = 2(1 - 4r^2)\mathbf{e}_z + \delta\mathbf{e}_y, \quad (3.1)$$

adding a finite-amplitude crosswise velocity of magnitude δ .

The perturbation (3.1) distorts the flow, nudging it towards the y -direction. A perturbation value of $\delta = 0.001$ is applied in the following simulations. For the sudden expansion pipe, this is the value of δ for which most results are presented in Sanmiguel-Rojas & Mullin (2012). Results were found to be compatible with the imperfections found in experiments. Figure 3(a-c) shows cross-sections of the pipe at $z = 22.5$ and presents contours of the axial velocity. Figure 3(a) is at $Re = 1000$ where the flow remains almost axisymmetric. For $Re = 1600$, figure 3(b) shows an asymmetry and can just be identified by comparing the solid and dashed lines. To see more clearly the effect of perturbation on the flow, the perturbed flow is subtracted from the (unperturbed) base flow, where it can be observed in the contour plot, figure 3(c), that the flow is accelerated on the right-hand side of the pipe section and decelerated on the opposite side. The applied perturbation at the inlet creates a recirculation region with a biased extent (see figure 3(d)). The reattachment pattern is very sensitive to the form of the perturbation given at the inlet, which motivates the application of a simple form of disturbance.

The asymmetry growth of the flow in the cross-section at $z = 22.5$ is measured by calculating the distance of the position of the peak axial velocity component from the centre of the pipe. The square of this distance is denoted ε (Mullin *et al.* (2009)). Figure 4(a) shows ε as a function of Re with least-square fit on the data obtained. It can be seen that at low Re there is no variation in the position of the centroid, a steady symmetric state is observed for $Re < 912$. As Re increases, a symmetry-breaking bifurcation occurs at a critical $Re_c = 912$. This value is smaller than the case of sudden expansion pipe

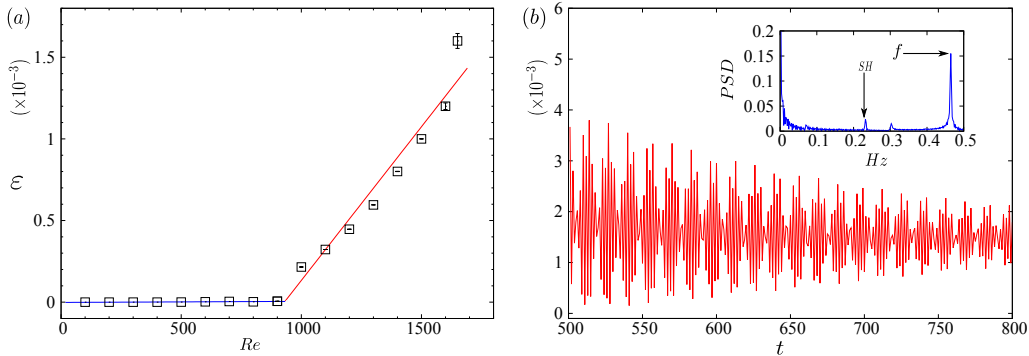


FIGURE 4. (a) Asymmetry growth of the flow measured by the square of the distance of the centroid from the centre of the pipe, ε , as a function of Re . The lines are least-square fit of the data and the intersection of the lines is at $Re_c = 912$ for the estimate of symmetry breaking bifurcation point. (b) Oscillations of ε at $Re = 1650$ as a function of time. The inset is the fast Fourier transform of the signal with a fundamental frequency $f = 0.468$ and a period doubling sub-harmonic $SH = 0.234$.

($Re_c = 1139$ in the experiment by Mullin *et al.* (2009)). Clearly, the critical Re depends on α and δ . The value of ε increases linearly ($912 < Re < 1500$) forming a steady asymmetric state, with biased growth in the recirculation region. The magnitude of the symmetry deviation grows as the square root of Re , typical of supercritical bifurcation. At larger Re an oscillation state arises ($1500 \leq Re \leq 1650$), and the flow becomes time dependent, due to the spatio-temporal oscillation of the reattachment point downstream (Sreenivasan & Strykowski 1983). The error bars in figure 4(a) represent the amplitude of the fluctuations in ε . These oscillations are also observed in experiments of sudden expansion flow (Mullin *et al.* 2009). When $Re = 1650$, the flow experiences quasi-periodic oscillations in the shear layer around the recirculation region. It can be seen in the velocity components along the axial as well as in the crosswise direction, and also in the ε evolution (see figure 4(b)). A fast Fourier transform (FFT) was performed on the signal to identify the dominant frequency. The inset in figure 4(b) is the FFT of the signal as a function of frequency, where $f = 0.468$ and $SH = 0.234$ a period doubling sub-harmonic. f seems to correspond to the frequency of vortex shedding around a circular or spherical body which occurs due to the Kelvin-Helmholtz instability (Fabre *et al.* 2008; Bobinski *et al.* 2014). This frequency of oscillation depends upon the type of the perturbation added to the system (Marquet *et al.* 2008; Ehrenstein & Gallaire 2009).

Figure 5(a) shows the friction coefficient, C_f , as a function of Re , computed on the wall of the outlet section. At low Re , the flow is steady and asymmetric and the value of C_f decreases. A significant contributor to the low values of C_f is that the present flow includes the recirculation region, which extends up to approximately half the of the outlet section before transition. Around the transition Reynolds number, $Re_t \simeq 1680$, the recirculation region inside the pipe breaks and leads to a localised turbulent state, shown in figure 5(b).

An important feature of the turbulence observed here is that it remains spatially localised at a constant position as observed in sudden expansion pipe flows (Sreenivasan & Strykowski 1983; Sanmiguel-Rojas & Mullin 2012). The formation of turbulence, near the diverging section, increases C_f due to higher internal mixing and resulting shear at the boundary. In this regime, C_f values scale roughly with the same exponent as the Blasius friction law, even though straight pipe flow are not turbulent at these Re . The present calculations for the perturbed flow were run up to $t = 600$ and the localised turbulence

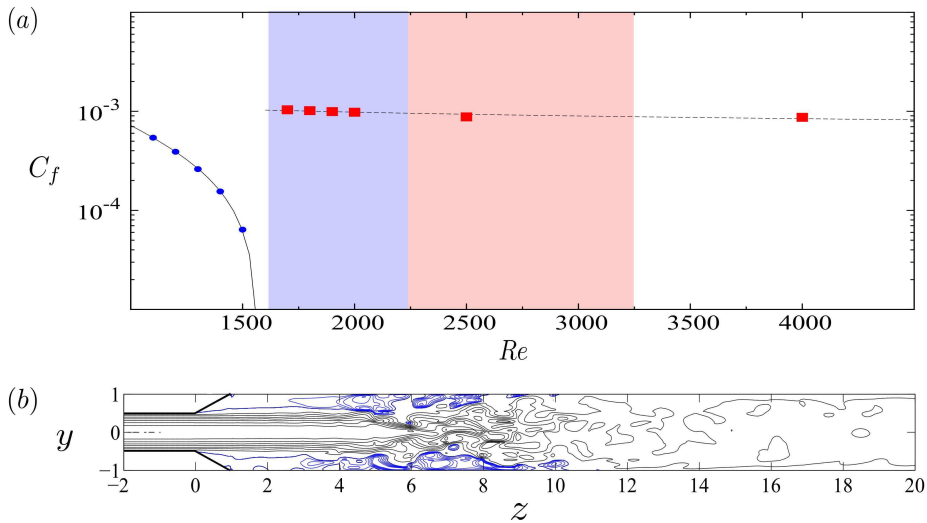


FIGURE 5. (a) Plot of friction coefficient, C_f , with respect to Re . The (blue) filled-circles represent the steady laminar asymmetric flow, the (red) filled-squares represent unsteady localised turbulent state. The continuous line represents the fit for the laminar state: $C_f = 1.97/Re - 0.0012$ and the dotted line represents a fit for localised turbulent state: $C_f = 0.0066(Re \times E)^{-0.22}$. The shaded regions $1650 \lesssim Re \lesssim 3273$ is the co-existence regime (hysteresis for $\delta = 0$), where the blue/dark subregion indicates the extent of the regime explored on the laminar branch in the present system. (b) Contour plot of streamwise velocity of localised turbulence at $Re = 1680$ with $\delta = 0.001$.

remained present. The perturbation was then removed and the flow was simulated up to $t = 1200$. The turbulence was observed to be self-sustained, and to occupy the same spatial position. The blue shaded region in figure 5(a) shows the range of Re in which a laminar state as well as a turbulent state co-exist for $1650 \lesssim Re \lesssim 2200$ for the present computational domain. Simulation above $Re > 2200$ without perturbation produces a steady laminar flow with a recirculation region that extends close to or beyond the outlet section. We have therefore limited the range of Re for computation on the laminar branch. For the case of simulations with a perturbation, the amplified energy in the diverging section breaks the recirculation region, creating an early transition, forming localised turbulence, and the computation may be carried out for larger Re along the turbulent branch. Global stability analysis (Sanmiguel-Rojas *et al.* 2010) have revealed that the first bifurcation for the sudden expansion pipe occurs at $Re \gtrsim 3273$ above which natural transition can be expected without any added perturbation. Given the much larger computational cost and that we have already computed a range of Re where the laminar and turbulent flows co-exist, we have not pursued the linear instability.

Further relaminarisation simulations were performed, where localised turbulence was generated at $Re_0 = 2000$ and the decay to laminar flow observed for Re below Re_t . In figure 6(a), the spatio-temporal diagram shows a typical relaminarisation case. At $t = 0$, Re is reduced suddenly from $Re_0 = 2000$ to $Re_f = 1500$. Here, the localised turbulence detaches from the inlet section almost immediately, then convects downstream and simultaneously decays, which can be seen as the disappearance of the vortical structures (Sibulkin 1962; Sreenivasan 1982). The relaminarisation time, t_R , was obtained by monitoring the time taken for the total energy in the computational domain to fall below a threshold of 10^{-6} . Above $Re_f = 1500$ the turbulence leaves the computational domain before falling below the threshold. The figure 6(b) shown t_R as a function of Re_f . The

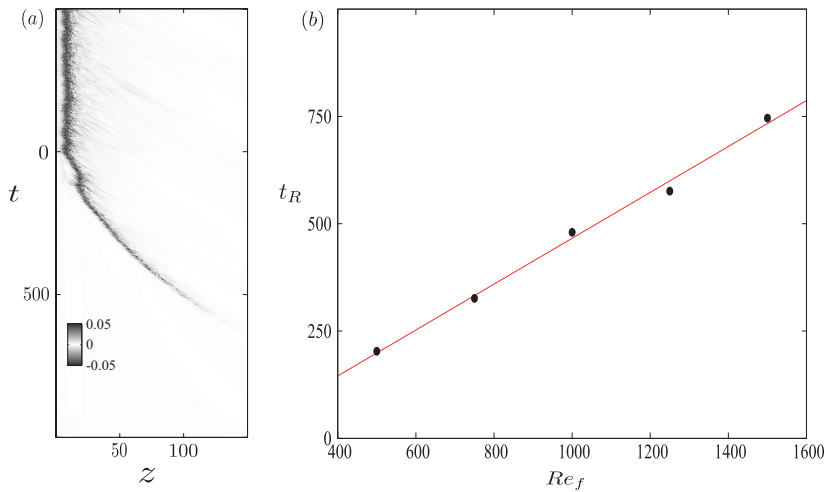


FIGURE 6. Relaminarisation study. (a) Spatio-temporal diagram of streamwise vorticity along the centreline of the pipe, where $z = 0$ corresponds to the start of the diverging section. The localised turbulence decays from $Re_0 = 2000$ to $Re_f = 1500$. (b) Relaminarization time, t_R , versus Re_f .

straight line fit indicates that the decay time of the turbulence increases linearly for $Re < 1500$, as identified in experiments (Peixinho & Besnard 2013). Here, no significant period of time was observed before the detachment of turbulence from the walls. Simulations were not carried out within the hysteresis region due to high computational cost. For these Re the turbulence is self-sustained for some time before detachment from the inlet section, and the time before detachment is expected to diverge rapidly as in uniform pipe flow (Avila *et al.* 2011).

Figure 7 shows the streamwise vorticity spatio-temporal diagram of simulations for (a) $Re = 4000$, (b) $Re = 3000$, (c) $Re = 2000$ and (d) $Re = 5000$, the horizontal axis represents the centre axis of the pipe from the diverging section to the outlet. The streamwise vorticity value has been normalised with the maximum vorticity and been plotted with the same scale for comparison purposes. It can be seen that for $Re = 2000$ the turbulence onsets at $t = 25$ and initially moves downstream, at $t = 100$ the turbulence starts moving upstream towards the diverging section and finally holds a stable position $z \simeq 10$. For $Re = 5000$, the onset of turbulence nearly occurs at the same time as that of $Re = 2000$, but the amount of time it takes to reach a localised position is $t = 40$, which is much smaller than that of the $Re = 2000$. The time taken to hold a stable position decreases as Re increases. The velocity trace downstream the localised turbulence for $Re = 2000$ recovers laminar flow (see figure 7(e)). Note that the Reynolds number based on the outlet diameter is half the value of Re . In the case of $Re = 5000$, the flow downstream the intense region of turbulence exhibits small patches of intense vorticity (see figure 7(d)). The streamwise velocity trace (see figure 7(f)) suggests weak turbulence, that does not return to laminar flow and eventually could lead to puff splitting (Avila *et al.* 2011; Shimizu *et al.* 2014). This property of expansion flow with laminar inlet profile forming localised turbulence and decaying in the outlet section is in good relation with experiments (Peixinho & Besnard 2013).

Structure within the localised turbulence is further studied using spatial correlations, which have been used to identify fast and slow streaks that dominate the coherent struc-

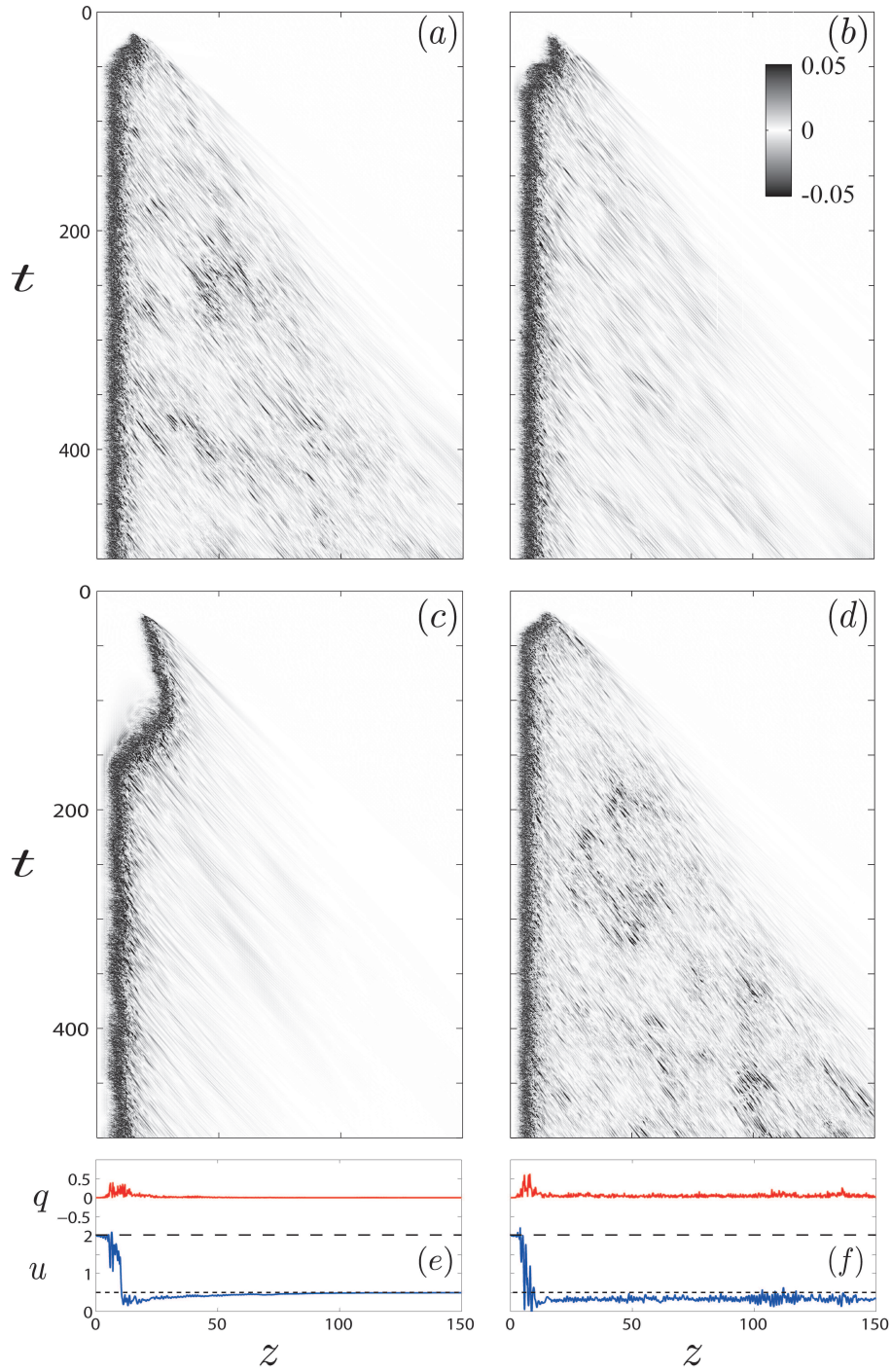


FIGURE 7. Evolution of localised turbulence. Spatio-temporal diagram of streamwise vorticity along the centreline of the pipe, where $z = 0$ corresponds to the start of the diverging section, for (a) $Re = 4000$, (b) $Re = 3000$, (c) $Re = 2000$ and (d) $Re = 5000$. (e) and (f) $q = \sqrt{v^2 + w^2}$ in (red) and streamwise velocity u (blue) at the final time step of (c) and (d). The dashed lines represent the Poiseuille centreline velocity in the inlet and the outlet sections.

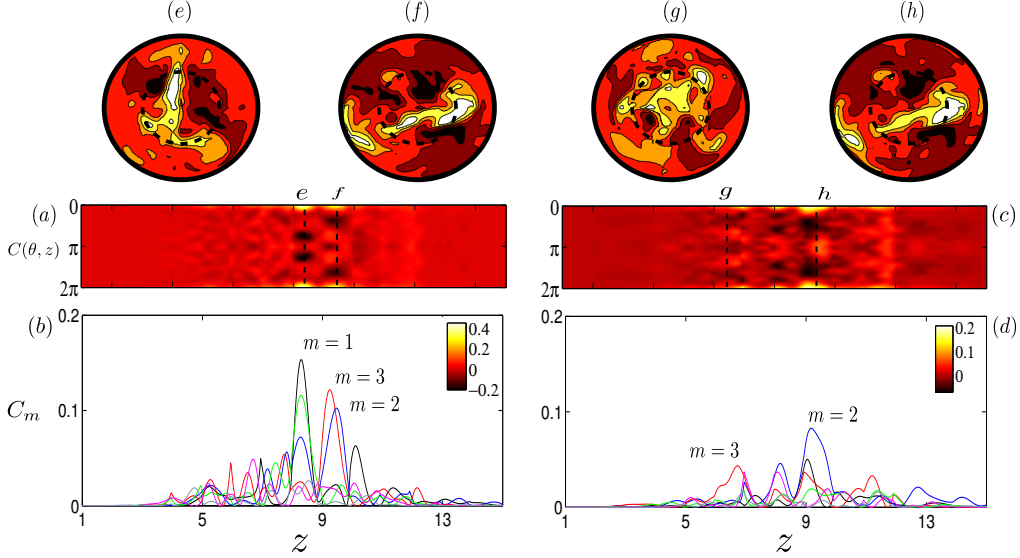


FIGURE 8. Spatial correlation on streamwise velocity of localised turbulence at $Re = 2000$. Contour of correlation, $C(\theta, z)$, at (a) $r = 0.5d$ and (c) $r = 0.8d$. Projection function of $C(\theta, z)$ for different azimuthal wave number m at (b) $r = 0.5d$ and (d) $r = 0.8d$. (e – h) Cross-sections of the axial flow relative to the time averaged profile with fast flow (light/white) and slow flow (dark/red) taken at the corresponding vertical dashed lines.

tures within puffs in pipe flow (Willis & Kerswell 2008). The correlation in the streamwise velocity is obtained using the function:

$$C(\theta, z) = \frac{2 \langle u_z(\theta + \phi, z) u_z(\phi, z) \rangle_\phi}{\langle \max(u_z)^2 \rangle_t} \Big|_r \quad (3.2)$$

where $\langle \cdot \rangle_s$ indicates averaging over the subscripted variable, u_z is the instantaneous axial flow velocity and r is the radial position. The signature of structures of a particular azimuthal wavenumber m is obtained by projecting the correlation function, $C_m(z) = 2 \langle C(\theta, z) \cos(m\theta) \rangle_\theta$ (Willis & Kerswell 2008). Figure 8(a,b) shows the correlation at $r = 0.5d$ and it can be seen that the $m = 1$ mode dominates the flow. Whereas in figure 8(c,d) at $r = 0.8d$, the $m = 2$ structure dominates the flow along with $m = 3$ with a much smaller correlation value, which suggests that the flow is more active in the centre region than near the wall. Overall this analysis points out that the localised turbulence in the gradual expansion possess a different flow structure from the turbulent puff (Wyganski & Champagne 1973; Shimizu & Kida 2009; Willis & Kerswell 2008) where $m = 3$ and 4 dominate the flow near the wall. The cross-sections in figure 8(e-h) indicate slow and fast moving flow.

4. Conclusions

Numerical results for the flow through a circular pipe with a gradual expansion in presence of an imperfection have been presented. The small imperfection leads to a linear asymmetry growth of the recirculation region, that has also been observed in experiments of sudden expansion pipe flow. As Re is increased, the long recirculation region oscillates seemingly due to shear Kelvin-Helmoltz instability (Sreenivasan & Strykowski 1983; Mullin *et al.* 2009). This time-dependent motion lies in a narrow range of Re for

the amplitude studied here ($\delta = 0.001$). With this level of imperfection, for $Re > 1680$ localised turbulence is triggered in the outlet section of the pipe. As undisturbed laminar flow ($\delta = 0$) is linearly stable up to at least $Re = 2200$, the small disturbance therefore provides a shortcut to subcritical turbulence. Due to the increasing length of the recirculation bubble, the critical Reynolds number for linear instability is beyond our computational limit. We observe that the triggered turbulence is self-sustained if the disturbance is removed. Hence, flow through a perfect gradual axisymmetric expansion ($\delta = 0$) exhibits multiplicity in the solution set of the Navier–Stokes equations, where both the axisymmetric laminar state and turbulent motion coexist over a substantial range of Re , from $Re \approx 1650$ up to the critical Reynolds number for linear instability. By comparison with the sudden expansion, we expect the critical Reynolds number approximately 3273 (Sanmiguel-Rojas *et al.* 2010). A hysteresis loop therefore exists, where for $\delta = 0$ transition to turbulence occurs at $Re_t \gtrsim 3273$ when Re is increased, and return to the laminar flow occurs at $Re \approx 1650$ when Re is decreased. The hysteresis range depends on the value of δ . Our simulations suggest that for $\delta = 0.001$ the hysteresis range is small ($1650 \lesssim Re \lesssim 1680$).

This property of localised turbulent flow with laminar inlet profile forming localised turbulence and decaying in the outlet section agrees with experiments (Sreenivasan & Strykowski 1983; Peixinho & Besnard 2013). The localised turbulence does not convect downstream but holds a stable spatial position. The structure within the localised turbulence is further studied using spatial correlations, which identifies fast and slow streaks that dominate the coherent structures. The main finding is that flow is more active in the centre region than near the wall. Hence, it is important to note that the localised turbulence observed here has different structure from that of a turbulent puff in uniform pipe flow (Willis & Kerswell 2008).

The authors acknowledge the financial support of the region Haute-Normandie and the computational time provided by CRIHAN. Our work has also benefited significantly from many helpful discussions with J.-C. Loiseau, J. E. Wesfreid and I. Mutabazi.

REFERENCES

- AVILA, K., MOXEY, D., DE LOZAR, A., AVILA, M., BARKLEY, D. & HOF, B. 2011 The onset of turbulence in pipe flow. *Science* **333** (6039), 192–196.
- BOBINSKI, T., GOUJON-DURAND, S. & WESFREID, J. E. 2014 Instabilities in the wake of a circular disk. *Phys. Rev. E* **89**, 053021.
- CANTWELL, C. D., BARKLEY, D. & BLACKBURN, H. M. 2010 Transient growth analysis of flow through a sudden expansion in a circular pipe. *Phys. Fluids* **22** (3), 034101.
- EHRENSTEIN, U. & GALLAIRE, F. 2009 Global low-frequency oscillations in a separating boundary-layer flow. *J. Fluid Mech.* **14**, 123–133.
- FABRE, D., AUGUSTE, F. & MAGNAUDET, J. 2008 Bifurcations and symmetry breaking in the wake of axisymmetric bodies. *Phys. Fluids* **20** (5), 051702.
- FISCHER, P., KRUSE, J., MULLEN, J., TUFO, H., LOTTES, J. & KERKEMEIER, S. 2008 nek5000: Open source spectral element CFD solver. <http://nek5000.mcs.anl.gov>.
- HAMMAD, K. J., ÖTÜGEN, M. V. & ARIK, E. B. 1999 A PIV study of the laminar axisymmetric sudden expansion flow. *Exp. Fluids* **26** (3), 266–272.
- LATORNELL, D. J. & POLLARD, A. 1986 Some observations on the evolution of shear layer instabilities in laminar flow through axisymmetric sudden expansions. *Phys. Fluids* **29** (9), 2828–2835.
- MADAY, Y., PATERA, A. T. & RØNQUIST, E. M. 1990 An operator-integration-factor splitting method for time-dependent problems: application to incompressible fluid flow. *J. Sci. Comput.* **5** (4), 263–292.

- MARQUET, O., SIPP, D., CHOMAZ, J.-M. & JACQUIN, L. 2008 Amplifier and resonator dynamics of a low-Reynolds-number recirculation bubble in a global framework. *J. Fluid Mech.* **605**, 429–443.
- MULLIN, T., SEDDON, J. R. T., MANTLE, M. D. & SEDERMAN, A. J. 2009 Bifurcation phenomena in the flow through a sudden expansion in a circular pipe. *Phys. Fluids* **21**, 014110.
- PEIXINHO, J. & BESNARD, H. 2013 Transition to turbulence in slowly divergent pipe flow. *Phys. Fluids* **25**, 111702.
- SANMIGUEL-ROJAS, E., DEL PINO, C & GUTIÉRREZ-MONTES, C 2010 Global mode analysis of a pipe flow through a 1:2 axisymmetric sudden expansion. *Phys. Fluids* **22** (7), 071702.
- SANMIGUEL-ROJAS, E. & MULLIN, T. 2012 Finite-amplitude solutions in flow through a sudden expansion in a circular pipe. *J. Fluid Mech.* **691**, 201–213.
- SHIMIZU, M. & KIDA, S. 2009 A driving mechanism of a turbulent puff in pipe flow. *Fluid Dyn. Res.* **41** (4), 045501.
- SHIMIZU, M., MANNEVILLE, P., DUGUET, Y. & KAWAHARA, G. 2014 Splitting of a turbulent puff in pipe flow. *Fluid Dyn. Res.* **46** (6), 061403.
- SIBULKIN, M. 1962 Transition from turbulent to laminar pipe flow. *Phys. Fluids* **5** (3), 280–284.
- SREENIVASAN, K. R. 1982 Laminarescent, relaminarizing and retransitional flows. *Acta Mec.* **44** (1-2), 1–48.
- SREENIVASAN, K. R. & STRYKOWSKI, P. J. 1983 An instability associated with a sudden expansion in a pipe flow. *Phys. Fluids* **26** (10), 2766–2768.
- WILLIS, A. P. & KERSEWELL, R. R. 2008 Coherent structures in localized and global pipe turbulence. *Phys. Rev. Lett.* **100** (124501).
- WYGNANSKI, I. J. & CHAMPAGNE, F. H. 1973 On transition in a pipe. Part 1. The origin of puffs and slugs and the flow in a turbulent slug. *J. Fluid Mech.* **59**, 281–335.